Supporting Information for "The importance of the inelastic and elastic structure of the crust in constraining glacial density, mass change, and isostatic adjustment from geodetic observations in southeast Alaska"

William Durkin[1], Samuel Kachuck[2,3], Matthew Pritchard[1]

[1]Earth and Atmospheric Sciences Department, Cornell University, Ithaca, New York, USA

[2]Department of Physics, Cornell University, Ithaca, New York, USA

[3]Department of Climate and Space Science and Engineering, University of Michigan, Ann Arbor, Michigan, USA

Contents

Corresponding author: William Durkin, `wjd73@cornell.edu`

1 Ice Mass Balance, SRTM Penetration Depth, and Uncertainties

1.1 Data and Methods

In this section, we provide the full description of the methods used to estimate ice thinning rates, the penetration depth of the Shuttle Radar Topography (SRTM) DEM, and mass balance estimates and uncertainties. We estimate ice mass balance using a weighted linear regression on a time series of stacked DEMs. These methods were developed by previous studies [e.g., *Nuimura et al.*, 2012; *Willis et al.*, 2012; *Melkonian et al.*, 2014; *Wang and Kääb*, 2015; *Berthier et al.*, 2016]. We construct an ice-elevation time series composed of SRTM, ArcticDEM, Advanced Spaceborne Thermal Emission and Reflection Radiometer (ASTER) DEMs. ASTER DEMs are downloaded pre-made by the NASA/USGS operated Land Process Distributive Active Archive Center(LDAAP), and cloudy images are manually removed. A total of 358 ASTER DEMs cover the study area, spanning July 2000 − May 2017 with an average of 15 ASTER elevations covering each pixel. ArcticDEM strips were derived from ∼0.5 m resolution stereoscopic imagery from Digital Globe and made available through the National Science Foundation and National Geospatial Intelligence Agency as 2 m resolution DEMs using the Surface Extraction with TIN-based Search-space Minimization (SETSM) method [https://www.pgc.umn.edu/data/arcticdem; *Noh and Howat*, 2015]. ArcticDEM strips covering the study area total in 401 DEMs that span the time period October 2008 − September 2016 with an average density of 2 ArcticDEM elevations per pixel. We downsample ArcticDEM strips to 30 m resolution and coregister both ArcticDEM and ASTER DEMs to off-ice pixels in the SRTM DEM using "PC_align" in the Ames Stereo Pipeline toolkit [*Moratto et al.*, 2010]. Off-ice pixels are identified using the Randolph Glacier Inventory version 5 [*Pfeffer et al.*, 2014]. Each DEM is assigned 1σ vertical uncertainty as the standard deviation between the off-ice pixels of it and the SRTM DEM. We estimate ice elevation change rates ($\frac{dh}{dt}$) using a linear regression on our elevation time series in which each elevation is weighted by the inverse of its uncertainty [e.g., *Melkonian et al.*, 2014; *Willis et al.*, 2012].

Outliers in the elevation time series are identified as those which deviate by an unrealistic amount from a reference DEM. Because the SRTM DEM is a radar product and is not affected by cloud coverage, it is often used as a reference elevation [e.g., *Willis et al.*, 2012; *Melkonian et al.*, 2014]. However, we begin by removing the SRTM DEM from our time series in order to investigate the SRTM penetration depth. Rather, we select the

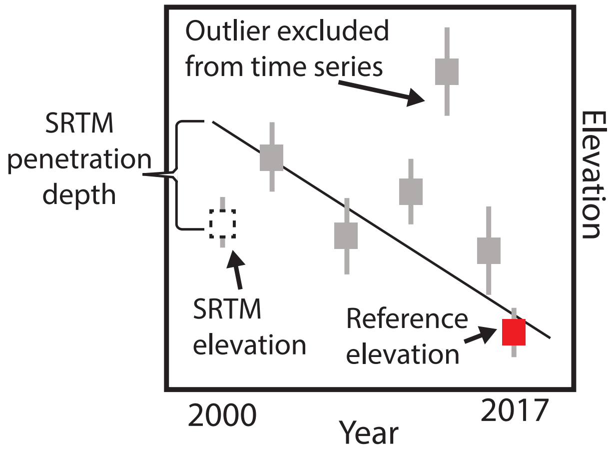

Figure 1. Cartoon showing SRTM C-Band penetration depth estimated with the "linear extrapolation" method. Squares and vertical lines show elevations with uncertainties in time series for a hypothetical location. The SRTM elevation (hatched square) is excluded from the time series, and the elevation with the minimum uncertainty (red square) is used as a reference to remove outliers from the time series. SRTM penetration depth is estimated from the difference between the extrapolated $\frac{dh}{dt}$ and SRTM DEM.

reference elevation on a pixel by pixel basis as the ASTER or ArcticDEM elevation in the time series with the minimum uncertainty ($\frac{dh}{dt}_{\sigma_{min}}$). For the Juneau Icefield, outliers in the time series are defined as elevations above a regional equilibrium line altitude of 1000 m [*Larsen et al.*, 2007] that deviate from the reference elevation by a rate exceeding $^{+5}_{-5}$ m yr^{-1} or $^{+5}_{-10}$ m yr^{-1} for elevations below 1000 m [e.g., *Melkonian et al.*, 2014]. For the Stikine Icefield, the threshold for elevations below 1000 m is changed to $^{+5}_{-30}$ m yr^{-1} [e.g., *Melkonian et al.*, 2016]. Because ArcticDEM and ASTER DEMs are derived from optical imagery, the quality of these data are heavily impacted by the high cloud coverage of the Glacier Bay region, and we are prevented from estimating $\frac{dh}{dt}_{\sigma_{min}}$ for this area due to insufficient DEM coverage. The root-mean-square error (RMSE) is calculated for each pixel, and pixels with an RMSE greater than the sum of the median and the median absolute deviation of the on-ice RMSE are removed. The approach of using elevation time series composed of optical-only imagery for the Juneau and Stikine icefields is similar to that of *Berthier et al.* [2018], but here includes the addition of the ArcticDEM dataset and the use of a reference elevation to exclude outliers from the time series.

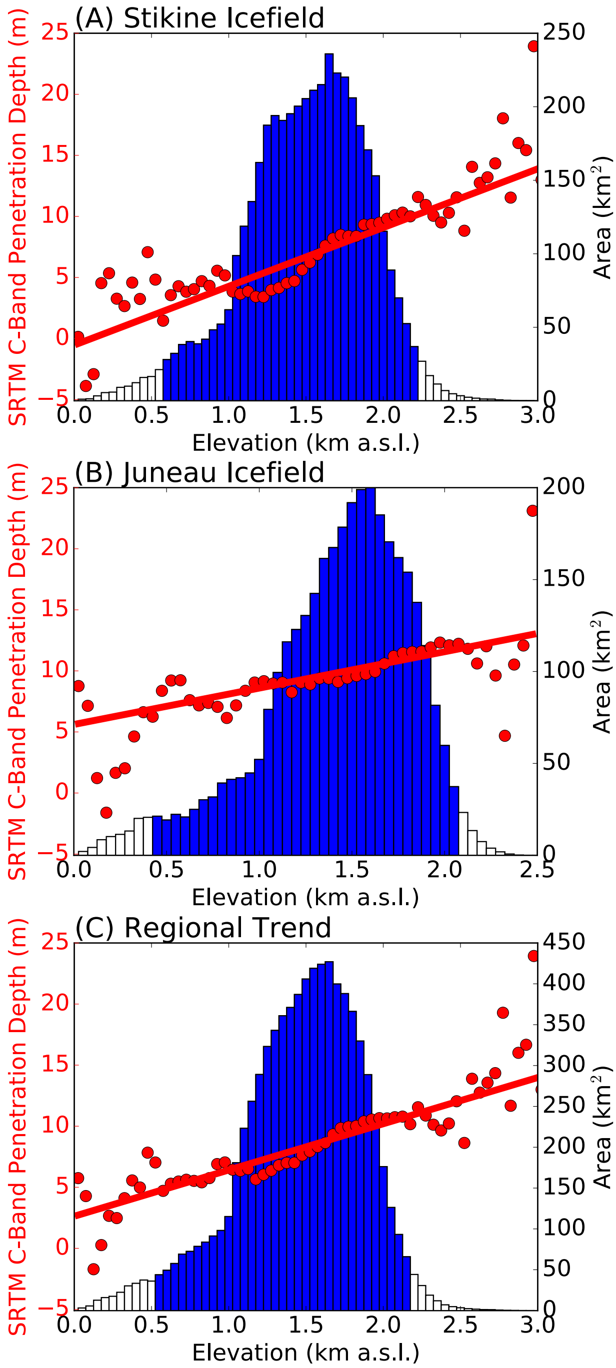

Figure 2. Elevation dependent penetration depth of the SRTM C-Band DEM estimated by linearly extrapolating a reference elevation to mid-February 2000 in 50 m elevation averaged bins (red dots). The elevation dependent trend (red line) is fit to the binned penetration depths within the center 95% of the icefields' area (shaded in blue) for (A) the Stikine Icefield, (B) the Juneau Icefield, and (C) the combined results of the Juneau and Stikine icefields (i.e., the "regional trend")

	SRTM C-Band Penetration Depth
Stikine Icefield	-0.53 m + 4.8 m per 1000 m a.s.l.
Juneau Icefield	5.61 m + 3.0 m per 1000 m a.s.l.
Regional Trend	2.63 m + 3.8 m per 1000 m a.s.l.

Table 1. Elevation dependent SRTM C-Band penetration depth trends for the Stikine Icefield, Juneau Icefield, and the regional trend (Supplementary Figure 2).

Following the methods of *Wang and Kääb* [2015] and *Berthier et al.* [2016], we linearly extrapolate the reference elevations to the acquisition date of the SRTM DEM (February 2000) using the $\frac{dh}{dt}_{\sigma_{min}}$, and estimate the SRTM C-band penetration depth as the difference from the SRTM DEM (Supplementary Figure 1). The elevation-dependent penetration depth is found by averaging the SRTM C-band penetration depth map into 50 m elevation bins and fitting a linear trend to the elevation band corresponding to the center 95% of each icefields' area. We calculate three elevation-dependent penetration depth corrections: for the combined Juneau and Stikine icefields (i.e. the "regional trend"), and for the Juneau and Stikine icefields separately (Supplementary Figure 2). We adjust SRTM elevations over the Juneau and Stikine icefields by adding each region's penetration depth trends over the appropriate area. SRTM elevations covering the Glacier Bay region are corrected using the regional trend. The corrected SRTM (SRTM*) is inserted into our elevation time series, $\frac{dh}{dt}$ is calculated using the SRTM* as a reference ($\frac{dh}{dt}_{SRTM^*}$), and outlying $\frac{dh}{dt}_{SRTM^*}$ values are removed using the RMSE filter. When estimating mass change rates, empty pixels in the $\frac{dh}{dt}_{SRTM^*}$ map are filled using the median of nearest pixels within a 1 km radius [e.g., *Melkonian et al.*, 2014]. Volume change rates are found by multiplying $\frac{dh}{dt}$ by pixel area, and mass change rates are estimated using a density of 850 ± 60 kg m^{-3} [e.g., *Huss*, 2013]. The improved estimates of the SRTM C-Band penetration depth, the extension of the ASTER time series by 3-8 years, and inclusion of the ArcticDEM in the $\frac{dh}{dt}_{SRTM^*}$ for the Juneau and Stikine icefields are an update to the results of *Melkonian et al.* [2014] and *Melkonian et al.* [2016].

Uncertainties due to DEM errors (σ_{DEM}) and density of material lost or gained (σ_ρ) are calculated following *Melkonian et al.* [2016], and we refer to the supplementary material of that study for detailed descriptions of the methods used. Because DEMs are not acquired at the same time each year, it is possible that the linear fit to a decadal trend may alias seasonal elevation variability. This uncertainty (σ_{season}) is estimated as the slope of the line that best fits the DEM acquisition times after they have been projected on to a simple sine wave seasonal elevation model with a uniform amplitude and period of one year [e.g., Figure 6 of *Berthier et al.*, 2016]. The amplitude of seasonal elevation variations is not well constrained for southeast Alaska, however *Berthier et al.* [2018] found that even with a large amplitude of 10 m, σ_{season} is an insignificant source of uncertainty for the Juneau and Stikine Icefields.

We estimate the effect that our asymmetric deviation threshold has on mass balance estimates (σ_{DEV}) by doubling the cutoff threshold of each icefield (i.e., $^{+10}_{-10}$ to $^{+10}_{-20}$ m yr^{-1} for Juneau and $^{+10}_{-10}$ to $^{+10}_{-60}$ m yr^{-1} for Stikine and the Glacier Bay region) and subtracting the resultant mass balance from our original mass balance estimates. Uncertainties associated with the SRTM correction are found for the Juneau and Stikine icefields by subtracting the mass balance derived from $\frac{dh}{dt}_{SRTM^*}$ with that of $\frac{dh}{dt}_{\sigma_{min}}$. For Glacier Bay, we do not have $\frac{dh}{dt}_{\sigma_{min}}$, so we take the trends found for separately for Juneau and Stikine as end members and calculate the difference from $\frac{dh}{dt}_{SRTM^*}$ found with the average trend. Ice mass balance uncertainty (σ_B) is calculated by adding sources of uncertainty listed above in quadrature.

$$\sigma_B = \sqrt{\sigma^2_{DEM} + \sigma^2_{season} + \sigma^2_{SRTM} + \sigma^2_{\rho} + \sigma^2_{DEV}} \quad (1)$$

1.2 Results

$\frac{dh}{dt}_{\sigma_{min}}$ is shown for Juneau and Stikine icefields in 50 m elevation-averaged bins in Supplementary Figure 4. After using $\frac{dh}{dt}_{\sigma_{min}}$ with the "linear extrapolation" technique [*Wang and Kääb*, 2015; *Berthier et al.*, 2016], we find the SRTM penetration depth, shown as 50 m elevation averaged bins for the Juneau and Stikine icefields (Supplementary Figure 2, Supplementary Table 1), with elevation dependent penetration depths of 5.6 m plus an additional 3.0 m penetration per 1000 m a.s.l. for Juneau and -0.53 m + 4.8 m per 1000 m a.s.l. for Stikine. The trend fitting the combined results of the two icefields (i.e., the "regional" trend) yields a penetration correction of 2.63 m + 3.8 m per 1000 m a.s.l. After applying the elevation dependent corrections to the SRTM and inserting the SRTM* into the elevation-time series, we find that the results of $\frac{dh}{dt}_{\sigma_{min}}$ and $\frac{dh}{dt}_{SRTM^*}$ on average agree to within 0.2 m yr $^{-1}$ (Supplementary Figure 4).

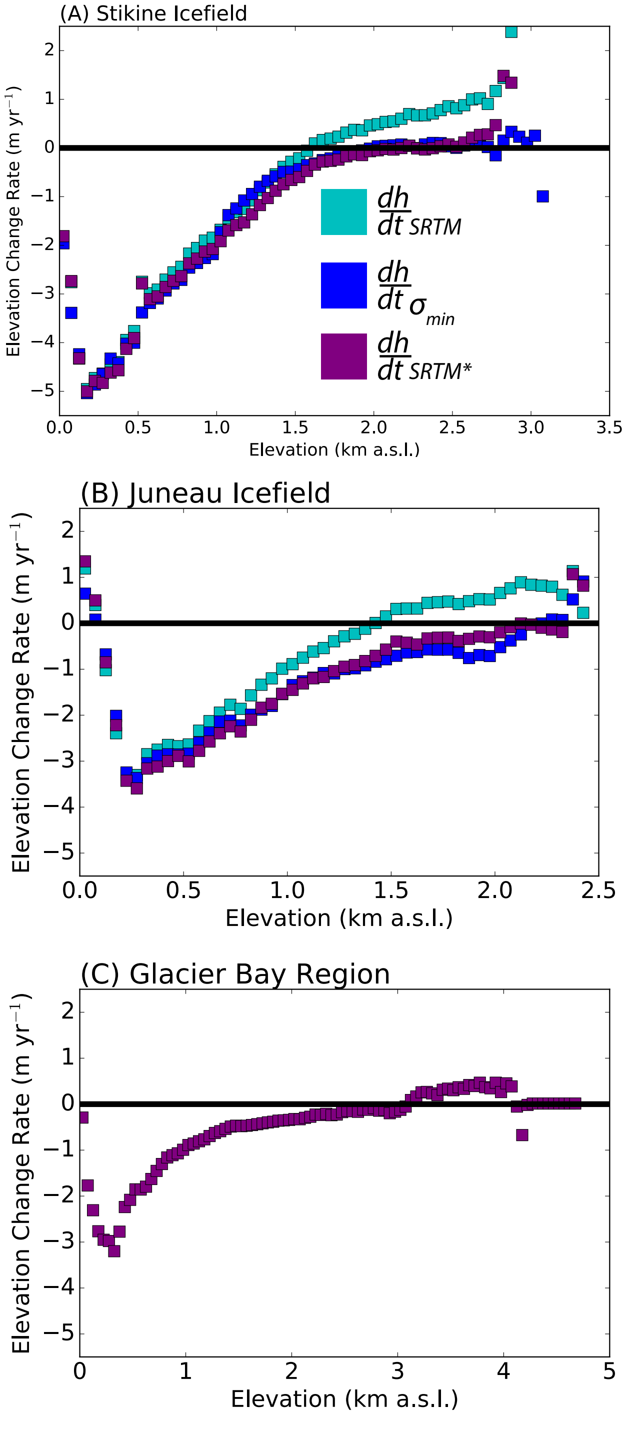

146 **Figure 3.** $\frac{dh}{dt}$ plotted against elevation for the Stikine Icefield (A), Juneau Icefield (B), and
147 Glacier Bay region (C). Three cases are shown for the Juneau and Stikine icefields: $\frac{dh}{dt}$ esti-
148 mated using the uncorrected SRTM DEM as the reference elevation (cyan), estimated using
149 only ASTER and ArcticDEM and referenced by the elevation with the lowest uncertainty (blue,
150 $\frac{dh}{dt}_{\sigma_{min}}$), and estimated using the corrected SRTM DEM as the reference (purple, $\frac{dh}{dt}_{SRTM*}$).
151 Following the correction applied to the SRTM DEM, $\frac{dh}{dt}_{SRTM*}$ agree to $\frac{dh}{dt}_{\sigma_{min}}$ within uncer-
152 tainty.

	$\frac{dh}{dt}_{\sigma_{min}}$ (m w.e. yr^{-1})	$\frac{dh}{dt}_{SRTM^*}$ (m w.e. yr^{-1})
Juneau Icefield	-0.85 ± 0.27	-0.75 ± 0.15
Stikine Icefield	-0.69 ± 0.12	-0.75 ± 0.08
Glacier Bay Region	—	-0.76 ± 0.11

Table 2. Mass balance estimates for Juneau Icefield, Stikine Icefield, and Glacier Bay region. In the first column, mass balance is estimated from ASTER and ArcticDEM-only elevation time series in which the elevation with the minimum uncertainty in the time series at each pixel is used as a reference to remove outliers (i.e., $\frac{dh}{dt}_{\sigma_{min}}$). In the second column, mass balances are estimated from corrected STRM (SRTM*), ASTER, and ArcticDEM elevation time series, and the SRTM* is used as a reference for removing outliers (i.e., $\frac{dh}{dt}_{SRTM^*}$)

Uncertainties for the mass balance calculations are summarized in Supplementary Table 2, and the size of each component of mass balance uncertainty is summarized in Supplementary Table 3. The amplitude of seasonal ice-elevation variations were not known a priori, and so we chose 10 m as an upper bound to adequately capture any real elevation amplitude [e.g., *Berthier et al.*, 2018]. For each of the three regions, although σ_{season} is similar to other sources of uncertainty, removing it from the uncertainty analysis would only change σ_B by about 1%.

Mass balance estimated using $\frac{dh}{dt}_{SRTM^*}$ for the Juneau Icefield (-0.75 ± 0.15 m w.e. yr^{-1}) and the Stikine Icefield (-0.75 ± 0.08 m w.e. yr^{-1}) agree within uncertainty to previous estimates based on an ASTER-only time series between years 2000-2016 [Juneau: -0.68 ± 0.15 m w.e. yr^{-1}; Stikine: -0.83 ± 0.12 m w.e. yr^{-1}; *Berthier et al.*, 2018], as well as with independent estimates based on LIDAR spanning years 1993-2013 [Juneau: -0.65 ± 0.22 m w.e. yr^{-1}; Stikine: -0.96 ± 0.28 m w.e. yr^{-1}; *Larsen et al.*, 2015]. Glacier Bay $\frac{dh}{dt}$ estimated using the "regional" correction for SRTM penetration depth is shown in Supplementary Figure 4. Using the SRTM penetration correction for the combination of Juneau and Stikine data, the Glacier Bay region has a mass balance of -5.26 ± 1.07 Gt yr^{-1}. *Johnson et al.* [2013] estimate the mass balance of the region using LIDAR data covering four time periods: 1995-2000 (-2.66±0.89 Gt yr^{-1}), 2000-2005 (-5.14 ± 1.27 Gt yr^{-1}), 2005-2009 (-2.96 ± 0.54 Gt yr^{-1}), and 2009-2011 (-6.06 ± 0.65 Gt yr^{-1}). If we take the average mass balance during the time periods 2000-2011 (the closest to the time period

	Juneau (Gt yr^{-1})	Stikine (Gt yr^{-1})	Glacier Bay (Gt yr^{-1})
σ_ρ Density	0.28	0.33	0.37
σ_{DEM} DEMs	0.08	0.09	0.08
σ_{DEV} Asymmetric Deviation	0.48	0.001	0.06
σ_{season} Aliasing Seasonal Changes	0.03	0.04	0.03
σ_{SRTM} SRTM C-Band Penetration	0.58	0.39	0.69

Table 3. Components of mass balance uncertainties used in Eq. 1. σ_ρ accounts for unknowns in the density of the glacial material lost or gained, σ_{DEM} for the uncertainty in the weighted linear regression applied to the elevation time series, and σ_{DEV} for the uncertainty due to the asymmetric cutoff threshold used to exclude outliers. σ_{season} represents uncertainties due to partially aliasing seasonal elevation variability in the DEM time series. Imperfect corrections for the SRTM C-Band penetration depth are (σ_{SRTM}) are estimated as the difference in mass balance estimates calculated from $\frac{dh}{dt}_{\sigma_{min}}$ and $\frac{dh}{dt}_{SRTM*}$. For the Glacier Bay region, σ_{SRTM} is calculated as the difference in mass balances estimated when applying the SRTM C-Band penetration trends found for the Juneau Icefield and Stikine Icefield to the Glacier Bay region.

covered in this study), the average estimated mass loss is -4.72 ± 1.52 Gt yr^{-1}, within the uncertainty of our estimate. If we allow the average mass loss during 2011-2017 to be the same as during the 2009-2011 period, the estimated ice mass loss during 2000-2017 becomes -5.06 ± 1.65 Gt yr^{-1}, strikingly similar to our own estimates. While we do note that the high intra-annual variability in mass balance observed by *Johnson et al.* [2013] makes a direct comparison to our results difficult, this provides a result from an independent dataset that is consistent with our findings.

1.3 Discussion

Previous estimates of SRTM C-Band penetration in southeast Alaska were estimated to be between 0-3 m based on the difference from the X-Band component of the SRTM, which was assumed to have small penetration into the snow and firn [*Melkonian et al.*, 2014]. This was a reasonable assumption at the time [e.g., *Gardelle et al.*, 2012], especially when considering the maritime environment and high water content of snow in southeast Alaska. *Dehecq et al.* [2016] and *Berthier et al.* [2016] found that the penetration

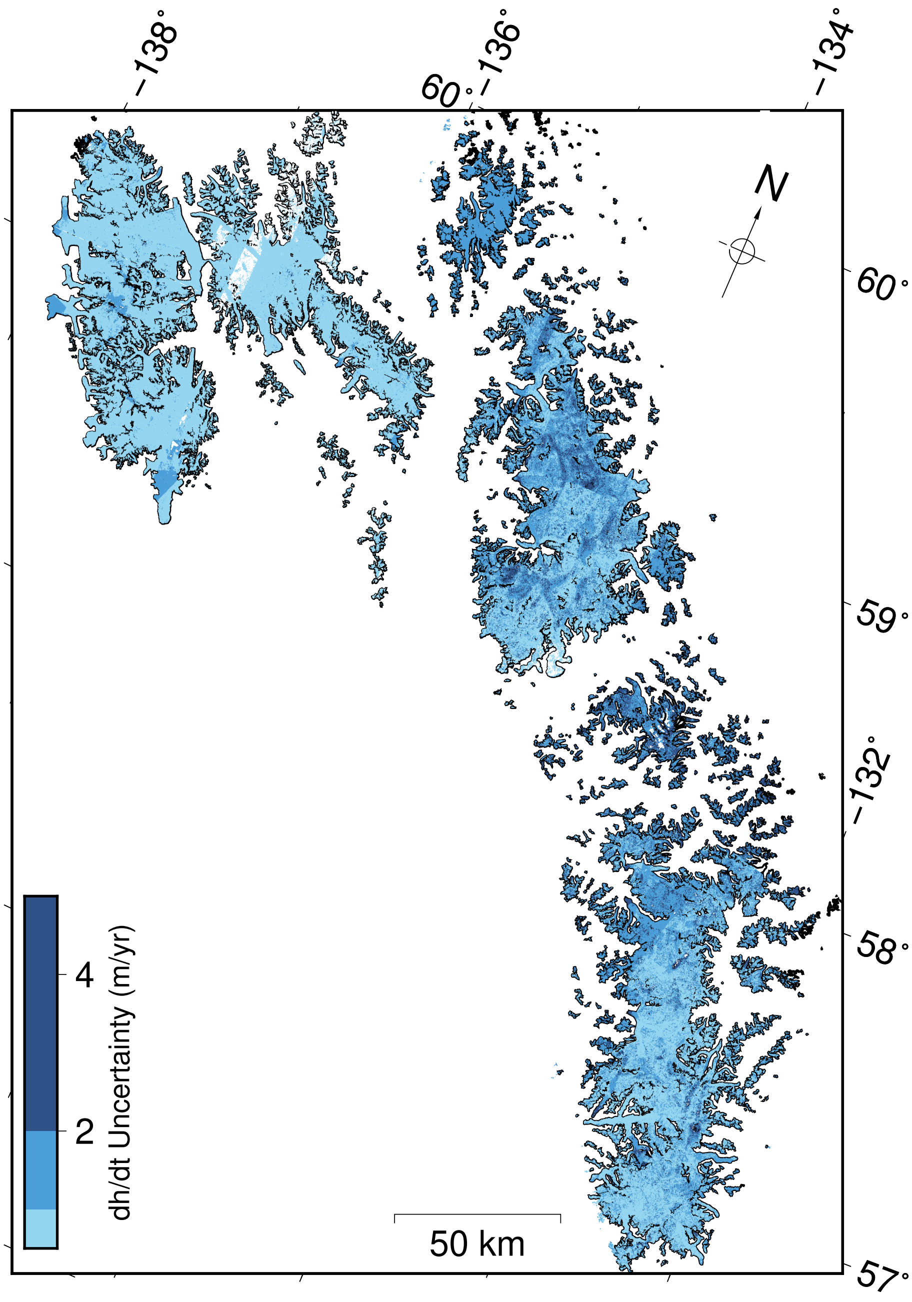

186 **Figure 4.** Uncertainties of $\frac{dh}{dt}_{SRTM*}$ based ice mass balance estimates (Supplementary Ta-
187 ble 3). Ice mass balance uncertainties are expressed as meters assuming a density of 850 kg m $^{-3}$.

depth of X-Band radar in the high-altitude, continental setting of the French Alps is on the order of 10 m, suggesting that the C-Band penetration depths based on an X-Band reference may similarly be underestimated. In light of this, *Melkonian et al.* [2016] accounted for the uncertainty in the C-Band penetration at the Stikine Icefield considered multiple scenarios, including a linear increase in penetration depth from 2-8 m between 1000 to 2500 m a.s.l.

By using an ASTER-only elevation time series, and eliminating the need to correct for a radar penetration depth, *Berthier et al.* [2018] found mass balance estimates for the Stikine Icefield more closely agreed to those found by *Melkonian et al.* [2016] under the 2-8 m SRTM-C Band penetration depth scenario than the 0-3 m penetration depth scenario. Similarly, *Berthier et al.* [2018] found that the 0-3m SRTM C-Band penetration depth correction results in overly positive mass balance estimates for the Juneau Icefield [*Melkonian et al.*, 2014], suggesting that the C-Band penetration depth in southeast Alaska may be similar to that of drier, continental settings. Here, we extend the discussion of *Berthier et al.* [2018].

While we do not estimate the SRTM's X-Band penetration depth explicitly, it may be inferred based on a comparison between our C-Band penetration depths and the SRTM C- and X-Band differences calculated in previous studies. *Melkonian et al.* [2014] found a difference between the SRTM X- and C- bands of $0-3$ m between the elevations of 700 to 1650 (i.e., 3.15 m of difference per 1000 m a.s.l.). This is consistent with our finding of a SRTM C-band penetration gradient of 3.0 m per 1000 m a.s.l. (Supplementary Figure 2, Supplementary Table 1). The difference between the SRTM C- and X-band DEMs are zero below 700 m a.s.l. [e.g., *Melkonian et al.*, 2014], where we find the consistent gradient in the C-band penetration. This implies that the X- and C-band of SRTM both have the same penetration depth and gradient, and that the X-band penetration gradient for elevations above 700 m is negligibly small for the Juneau Icefield. In other words, the SRTM X-band penetration depth of the Juneau Icefield is not constant, ranging between 2.25-7.86 m at 750 m a.s.l and appears to remain at this value for higher elevations. For the Juneau Icefield, Stikine Icefield, and the regional fit, we find mean SRTM C-band penetration depths of 7.3-10.3 m, in agreement with the penetration depths found in the French Alps of 8-9 m [*Berthier et al.*, 2016].

To compare our regional penetration depth estimates against estimates made from independent datasets, we consider the results of *Larsen et al.* [2007] who corrected the C-band penetration of SRTM as well as seasonal elevation differences between February and August 2000 by comparing 12 LIDAR surveys made over the Yakutat, Glacier Bay, Juneau Icefield, and Stikine Icefield regions in August 2000. *Larsen et al.* [2007] found an elevation dependent penetration depth of -2.5 m + 2.6 m per 1000 m a.s.l, ~30% lower than the penetration gradient we find for our regional fit. The linear trend fit by *Larsen et al.* [2007] to the difference between the LIDAR surveys and the SRTM DEM spans elevations between 500-1700 m a.s.l. This corresponds to about 68% of the combined Juneau and Stikine icefields' area, whereas our study focuses on the center 95% of the icefields' area, corresponding to elevation bands of 525-2125 m a.s.l. When we fit a trend to the 500-1700 m a.s.l. elevation band for the regional combination, we find a penetration trend of 3.74 m + 2.6 m per 1000 m a.s.l. The agreement in the 2.6 m per 10000 m a.s.l SRTM C-band penetration gradient found here when fitting to the same elevation band provides an independent validation of the linear extrapolation method for southeast Alaska.

2 Load Love Number Summary

As a benchmark for loading Love numbers calculated with giapy [*Kachuck*, 2018], Love numbers for PREM are shown in Supplementary Figure 5 for both `giapy` and those calculated by *Melini et al.* [2015]. Further benchmarking of `giapy` is detailed in *Kachuck* [2018]. Supplementary Figure 6 shows the load Love numbers calculated for each of the 42 elastic structures in our ensemble.

3 Impact of Disc Size on Elastic Deformation

Supplementary Figure 7 shows the elastic uplift rates modeled using the PREM elastic structure with $\frac{dh}{dt}$ sampled at 0.01° (1.11 km), 0.005° (556 m), and 0.0025° (228 m) resolutions using the nearest neighbor method. The larger uplift rates found when 0.01° diameter discs are used are the result of the bias in the $\frac{dh}{dt}$ distribution when ice thinning rates are sampled at this resolution (Section 3.2 of the main text). Elastic uplift rates modeled with 0.005° diameter discs agree to within 5% of uplift rates modeled with 0.0025° diameter discs. Using 0.01° diameter discs over estimates the elastic uplift rates in both the near- and far-fields, resulting in a 30% increase in elastic uplift rates at 500 m from the nearest ice covered area and a 50% increase at 50 km distance from the ice in

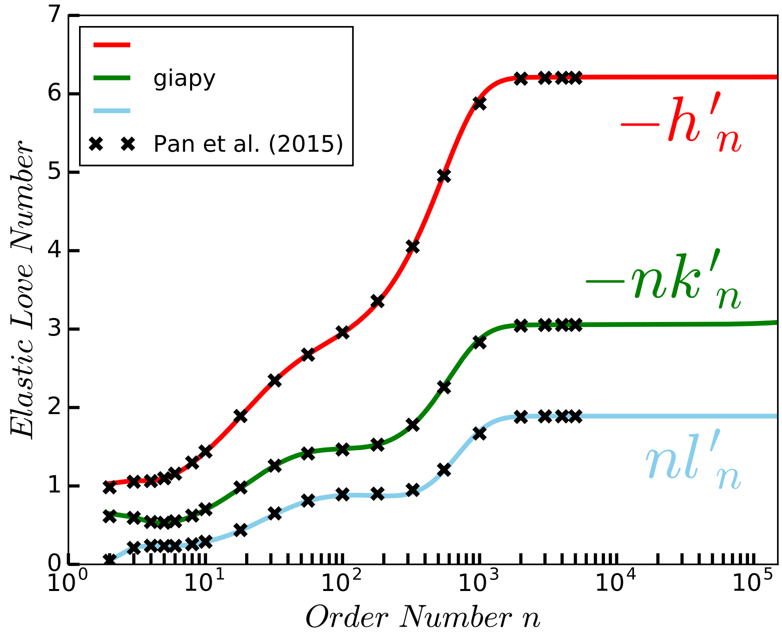

256 **Figure 5.** Elastic load Love number solutions l'_n (blue), k'_n (green), and h'_n (red) for the
257 PREM Earth structure [*Dziewonski and Anderson*, 1981] computed to a harmonic degree of
258 150,000 using giapy [*Kachuck*, 2018]. Black crosses show the load Love number solutions to
259 PREM provided by *Pan et al.* [2015] to a harmonic order of 6,000.

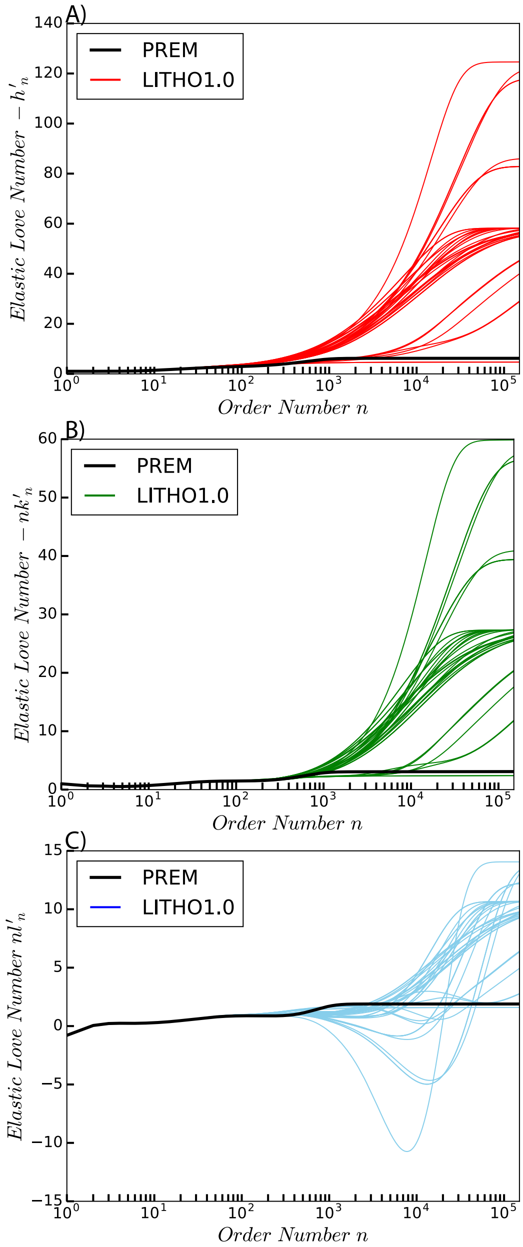

Figure 6. Elastic load Love numbers h$'_n$, k$'_n$ (B), and l'_n (C) calculated to a harmonic order of 150,00 for each model in the ensemble of LITHO1.0 [*Pasyanos et al.*, 2014]. Load Love numbers calculated for PREM are shown in black.

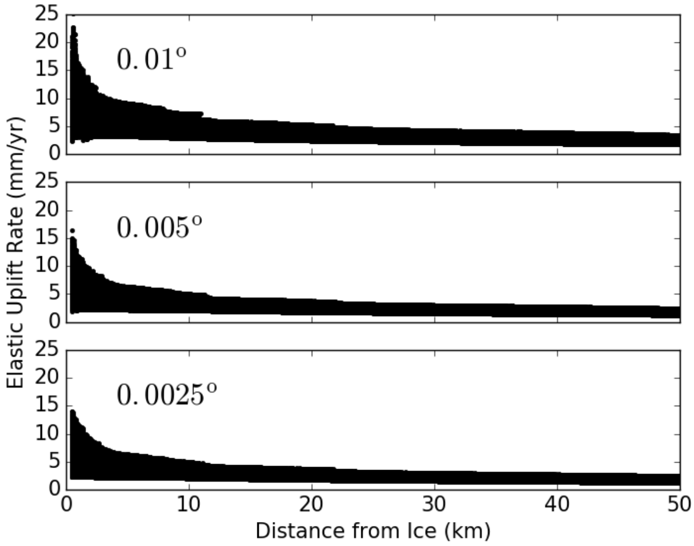

Figure 7. Scatter plots of elastic uplift rates of all gridded points in the study region plotted against their distance to the nearest ice covered area. Elastic uplift rates are modeled from the ensemble of LITHO1.0 elastic structures using discs of 0.01°, 0.005°, and 0.0025° diameter. Uplift rates modeled using 0.01° are positively biased due to the overly-negative ice mass balance estimates that results from sampling $\frac{dh}{dt}$ at this resolution (see section 3.2 of the main text).

comparison to the elastic uplift rates modeled with 0.0025° diameter discs (Supplementary Figure 7). As discussed in section 3.2 of the main text, load Love numbers used to model elastic deformation were calculated to a harmonic degree of 150,000. The harmonic degree (n) needed to resolve deformation resulting from a load of radius α is given by *Jeans* [1923] as

$$n = \frac{360}{\alpha} \qquad (2)$$

Thus a disc of 0.005° diameter should be modeled using load Love numbers calculated to a harmonic degree of at least 144,000 and at least 288,000 for a 0.0025° diameter disc. *Bevis et al.* [2016] suggest that this rule may be judiciously violated in order to avoid excessive computing time costs. The close agreement between elastic deformation modeled using 0.005° and 0.0025° diameter discs (Supplementary Figure 7) indicates that a harmonic degree of 150,000 is sufficiently high for this study.

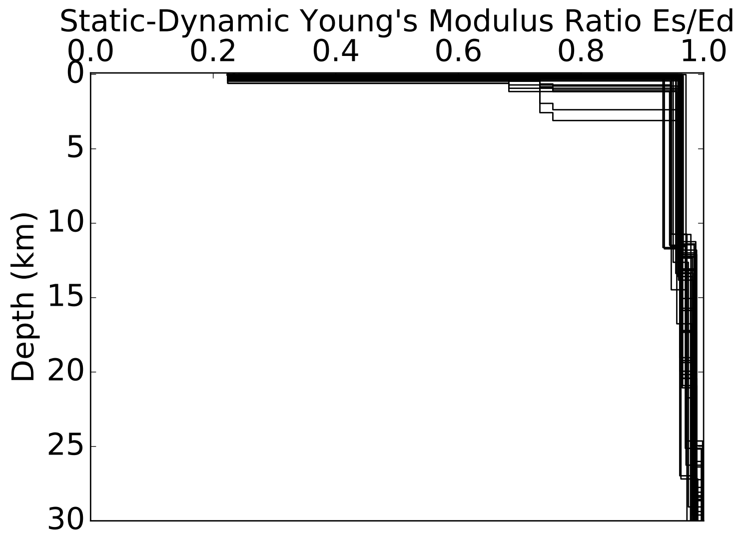

Figure 8. Static-dynamic Young's modulus ratios (E_S/E_D) calculated from Eq. 1 of the main text for each of the 42 LITHO1.0 elastic structures.

4 Static-Dynamic Ratio

The inelastic corrections described in Eq. 1 of the main text are based on laboratory experiments conducted at a narrow range of confining pressures 0–100 MPa,or the upper 5 km of the crust [*Yale et al.*, 2017]. However, as confining pressures increase, pores and fractures close and the static-dynamic ratio of a rock approaches 1 at depths of ∼12-15 km [*Cheng and Johnston*, 1981]. We must take care that applying Eq. 1 of the main text to the LITHO1.0 ensemble does not yield static-dynamic ratios that are implausibly small at too great of depths. Supplementary Figure 8 shows the scaling factor plotted against depth for each of the 42 LITHO1.0 structures. At a depth of 3.1 km, the smallest E_S/E_D in the ensemble is 0.75 to 0.90, and beyond depths of 10 km is no lower than 0.95. This is consistent with the E_S/E_D of 0.9 found by *Cheng and Johnston* [1981] for granite at confining pressures equivalent to depths of 12-13 km. Differences between the static and dynamic moduli of less than 5% at depths beyond 10 km are negligibly small for the purposes of this study.

References

Berthier, E., V. Cabot, C. Vincent, and D. Six (2016), Decadal Region-Wide and Glacier-Wide Mass Balances Derived from Multi-Temporal ASTER Satellite Digital Elevation Models. Validation over the Mont-Blanc Area, *Frontiers in Earth Science*, *4*(June), 1–16, doi:10.3389/feart.2016.00063.

Berthier, E., C. Larsen, W. J. Durkin, M. J. Willis, and M. E. Pritchard (2018), Brief communication: Unabated wastage of the Juneau and Stikine icefields (southeast Alaska) in the early 21st century, *The Cryosphere*, *12*(4), 1523–1530, doi:10.5194/tc-12-1523-2018.

Bevis, M., D. Melini, and G. Spada (2016), On computing the geoelastic response to a disk load, *Geophysical Journal International*, *205*(3), 1804–1812.

Cheng, C., and D. H. Johnston (1981), Dynamic and static moduli, *Geophysical Research Letters*, *8*(1), 39–42.

Dehecq, A., R. Millan, E. Berthier, N. Gourmelen, E. Trouvé, and V. Vionnet (2016), Elevation changes inferred from TanDEM-X data over the Mont-Blanc area: Impact of the X-band interferometric bias, *IEEE Journal of Selected Topics in Applied Earth Observations and Remote Sensing*, *9*(8), 3870–3882.

Dziewonski, A. M., and D. L. Anderson (1981), Preliminary reference earth model, *Physics of the earth and planetary interiors*, *25*(4), 297–356.

Gardelle, J., E. Berthier, and Y. Arnaud (2012), Slight mass gain of Karakoram glaciers in the early twenty-first century Slight mass gain of Karakoram glaciers in the early twenty-first century, *Nature Geoscience*, *5*(5), 1–4, doi:10.1038/ngeo1450.

Huss, M. (2013), Density assumptions for converting geodetic glacier volume change to mass change, *The Cryosphere*, *7*(3), 877–887.

Jeans, J. H. (1923), The propagation of earthquake waves, *Proc. R. Soc. Lond. A*, *102*(718), 554–574.

Johnson, A. J., C. F. Larsen, N. Murphy, A. A. Arendt, and S. Lee Zirnheld (2013), Mass balance in the Glacier Bay area of Alaska, USA, and British Columbia, Canada, 1995-2011, using airborne laser altimetry, *Journal of Glaciology*, *59*(216), 632–648, doi:10.3189/2013JoG12J101.

Kachuck, S. (2018), Time-domain glacial isostatic adjustment: theory, computation, and statistical applications, Ph.D. thesis, Cornell University.

Larsen, C. F., R. J. Motyka, A. A. Arendt, K. a. Echelmeyer, and P. E. Geissler (2007), Glacier changes in southeast Alaska and northwest British Columbia and contribution to sea level rise, *Journal of Geophysical Research: Earth Surface*, *112*(1), 1–11, doi:10.1029/2006JF000586.

Larsen, C. F., E. Burgess, A. A. Arendt, S. O'Neel, A. J. Johnson, and C. Kienholz (2015), Surface melt dominates Alaska glacier mass balance, *Geophysical Research Letters*, *42*(14), 5902–5908, doi:10.1002/2015GL064349.

Melini, D., P. Gegout, O. Midi-Pyrenees, and G. Spada (2015), a regional elastic rebound calculator.

Melkonian, A. K., M. J. Willis, M. E. Pritchard, a. Rivera, F. Bown, and S. A. Bernstein (2014), Satellite-derived volume loss rates and glacier speeds for the Cordillera Darwin Icefield, Chile, *Cryosphere*, *7*(3), 823–839, doi:10.5194/tc-7-823-2013.

Melkonian, A. K., M. J. Willis, and M. E. Pritchard (2016), Stikine Icefield Mass Loss between 2000 and 2013/2014, *Frontiers in Earth Science*, *4*(October), doi:10.3389/feart.2016.00089.

Moratto, Z., M. Broxton, R. Beyer, M. Lundy, and K. Husmann (2010), Ames Stereo Pipeline, NASA's open source automated stereogrammetry software, in *Lunar and Planetary Science Conference*, vol. 41, p. 2364.

Noh, M. J., and I. M. Howat (2015), Automated stereo-photogrammetric DEM generation at high latitudes: Surface Extraction with TIN-based Search-space Minimization (SETSM) validation and demonstration over glaciated regions, *GIScience and Remote Sensing*, *52*(2), 198–217, doi:10.1080/15481603.2015.1008621.

Nuimura, T., K. Fujita, S. Yamaguchi, and R. R. Sharma (2012), Elevation changes of glaciers revealed by multitemporal digital elevation models calibrated by GPS survey in the Khumbu region, Nepal Himalaya, 1992-2008, *Journal of Glaciology*, *58*(210), 648–656.

Pan, E., J. Chen, M. Bevis, A. Bordoni, V. R. Barletta, and A. Molavi Tabrizi (2015), An analytical solution for the elastic response to surface loads imposed on a layered, transversely isotropic and self-gravitating earth, *Geophysical Supplements to the Monthly Notices of the Royal Astronomical Society*, *203*(3), 2150–2181.

Pasyanos, M. E., T. G. Masters, G. Laske, and Z. Ma (2014), LITHO1.0: An updated crust and lithospheric model of the Earth, *Journal of Geophysical Research: Solid Earth*, *119*(3), 2153–2173.

Pfeffer, W. T., A. A. Arendt, A. Bliss, T. Bolch, J. G. Cogley, A. S. Gardner, J.-O. Hagen, R. Hock, G. Kaser, C. Kienholz, et al. (2014), The Randolph Glacier Inventory: a globally complete inventory of glaciers, *Journal of Glaciology*, *60*(221), 537–552.

Wang, D., and A. Kääb (2015), Modeling Glacier Elevation Change from DEM Time Series, *Remote Sensing*, *7*(8), 10,117–10,142, doi:10.3390/rs70810117.

Willis, M. J., A. K. Melkonian, M. E. Pritchard, and A. Rivera (2012), Ice loss from the Southern Patagonian Ice Field, South America, between 2000 and 2012, *Geophysical research letters*, *39*(17).

Yale, D., V. Swami, et al. (2017), Conversion of Dynamic Mechanical Property Calculations to Static Values for Geomechanical Modeling, in *51st US Rock Mechanics/Geomechanics Symposium*, American Rock Mechanics Association.